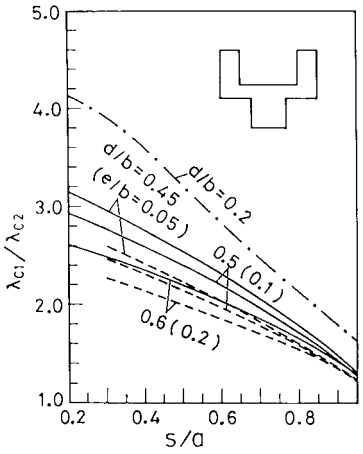

(a)

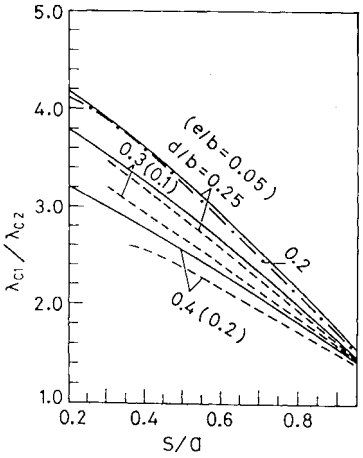

(b)

Fig. 6. Bandwidth $\lambda_{c1}/\lambda_{c2}$ versus s/a. All parameters and denotations as in Fig. 5. (a) $h/b = 0.4$ and (b) $h/b = 0.2$.

the SRG bandwidth, but the cutoff wavelength can be substantially larger. Thus, the properly designed RTW can be a broad-band low-impedance transmission medium. The RTW in the other configuration with a ridge wider than the trough appears less useful because the trough lowers both the cutoff wavelength and bandwidth.

References

[1] K. E. Jones, E. W. Strid, and K. R. Gleason, "Mm-wave wafer probes span 0 to 50 GHz," *Microwave J.*, vol. 30, no. 4, pp. 177–183, 1987.

[2] G. Begemann, "An X-band balanced finline mixer," *IEEE Trans. Microwave Theory Tech.*, vol. MTT-26, pp. 1007–1011, 1978.

[3] J. V. Bellantoni, R. C. Compton, and H. M. Levy, "A new W-band coplanar waveguide text fixture," in *1989 IEEE MTT-S Int. Microwave Symp. Dig.*, pp. 1203–1204.

[4] G. E. Ponchak and R. N. Simons, "A new rectangular waveguide to coplanar waveguide transition," in *IEEE MTT-S Int. Microwave Symp. Dig.*, vol. I, Dallas, TX, May 8–10, 1990, pp. 491–493.

[5] E. M. Godshalk, "A V-band wafer probe using ridge-trough waveguide," *IEEE Trans. Microwave Theory Tech.*, vol. 39, pp. 2218–2228, Dec. 1991.

[6] R. N. Simons, "New channelised coplanar waveguide to rectangular waveguide post and slot couplers," *Elec. Lett.*, vol. 27, no. 10, pp. 856–857, 1991.

[7] R. N. Simons and S. R. Taub, "New coplanar waveguide to rectangular waveguide end launcher," *Elec. Lett.*, vol. 28, no. 12, pp. 1138–1139, June 4, 1992.

[8] J. P. Montgomery, "On the complete eigenvalue solution of ridged waveguide," *IEEE Trans. Microwave Theory Tech.*, vol. MTT-19, pp. 547–555, June, 1971.

[9] D. Dasgupta and P. K. Saha, "Eigenvalue spectrum of rectangular waveguide with two symmetrically placed double ridges," *IEEE Trans Microwave Theory Tech.*, vol. MTT-29, pp. 47–51, Jan. 1981.

[10] G. G. Mazumder and P. K. Saha, "A novel rectangular waveguide with double T-septums," *IEEE Trans. Microwave Theory Tech.*, vol. MTT-33, pp. 1235–1238, Nov. 1985.

[11] P. K. Saha and D. Guha, "New broadband rectangular waveguide with L-shaped septa," *IEEE Trans. Microwave Theory Tech.*, vol. 40, pp. 777–781, Apr. 1992.

Modal Scattering Matrix of the General Step Discontinuity in Elliptical Waveguides

Paweł Matras, Rainer Bunger, and Fritz Arndt

***Abstract*—In this paper, a direct mode-matching technique is proposed for the calculation of the modal scattering matrix of nonconfocal, twisted, and/or displaced step discontinuities in elliptical waveguides of different cross sections. For the convenient treatment of the Mathieu functions, an efficient trigonometric series expansion technique is used. As examples, the scattering parameters are calculated for typical step discontinuities demonstrating the flexibility of the method.**

***Index Terms*— Mode-matching methods, waveguide discontinuities, waveguide junctions.**

I. Introduction

For the analysis of the step discontinuity at elliptical waveguides, an efficient direct mode-matching technique has been recently proposed [5]. The investigation was limited to the simple case of confocal elliptic cross sections. The rigorous solution of the scattering problem at the general (nonconfocal, twisted, and/or displaced) discontinuity [see Fig. 1(a)], however, is required for the analysis of more complicated structures such as displaced elliptic irises or shaped horns. This paper presents, therefore, the extension of the direct mode-matching technique to this general case.

II. Theory

For a waveguide of elliptical cross section [cf. Fig. 1(b)] with the focal distance $2h$, the wave equation for the corresponding transversal eigenfunctions $T(\xi, \eta) = U(\xi)V(\eta)$ is given in elliptic coordinates ξ, η, z by [4]

$$\frac{\partial^2 V}{\partial \eta^2} + (a - 2q\cos 2\eta)V = 0 \tag{1}$$

$$\frac{\partial^2 U}{\partial \xi^2} - (a - 2q\cosh 2\xi)U = 0 \tag{2}$$

Manuscript received November 10, 1995; revised November 21, 1996.

The authors are with the Microwave Department, University of Bremen, D-28359 Bremen, Germany.

Publisher Item Identifier S 0018-9480(97)01730-4.

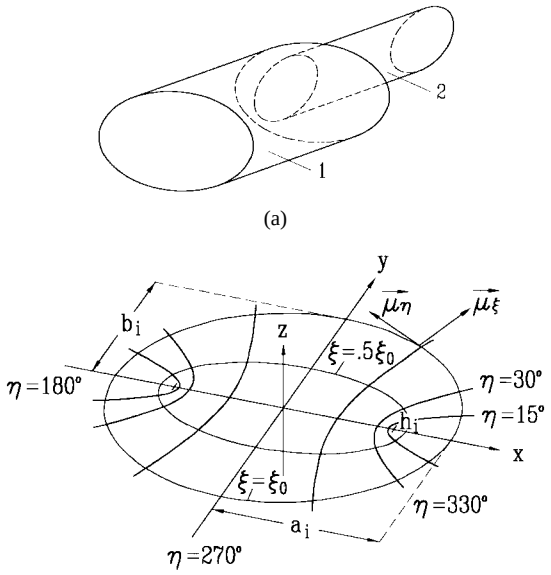

Fig. 1. General (nonconfocal, displaced, and twisted) step discontinuity at elliptical waveguides of different cross section. (a) General step discontinuity. (b) Elliptical coordinate system.

with the abbreviation

$$q = \frac{k_c^2}{4} h^2 \tag{3}$$

where k_c is the cutoff wavenumber and a is a constant, which is denoted as the "separation constant" [4].[1]

The formal solution of the eigenvalue problem (1) and (2) leads to [4]

$$T(\xi, \eta) = \begin{Bmatrix} \mathrm{Ce}(\xi)\mathrm{ce}(\eta) \\ \mathrm{Se}(\xi)\mathrm{se}(\eta) \end{Bmatrix} \tag{4}$$

where ce, se, and Ce, Se denote the even and odd Mathieu, and even and odd modified Mathieu functions, respectively. Equation (2) (the modified Mathieu equation), is related to (1) (the Mathieu equation), via the transformation $\xi = j\eta$, where $j = \sqrt{-1}$.

Equation (1) is solved by the following trigonometric series expansion of [2] and [7]:

$$\mathrm{ce}_{2n}(\eta) = \sum_{r=0}^{\infty} A_{2r} \cos(2r\eta) \tag{5}$$

$$\mathrm{ce}_{2n+1}(\eta) = \sum_{r=0}^{\infty} A_{2r+1} \cos[(2r+1)\eta] \tag{6}$$

$$\mathrm{se}_{2n+1}(\eta) = \sum_{r=0}^{\infty} B_{2r+1} \sin[(2r+1)\eta] \tag{7}$$

$$\mathrm{se}_{2n+2}(\eta) = \sum_{r=0}^{\infty} B_{2r+2} \sin[(2r+2)\eta]. \tag{8}$$

For the solution of (2), a Bessel function expansion is used for the modified Mathieu functions [1] and [7].

With (1)–(8), first the separation constant a in (1) and (2), and then the coefficients in (5)–(8) are determined numerically. For a, the equation

$$\begin{aligned} L(a) &= a - m^2 - u_m - v_m \\ &= 0, \qquad m \geq 0 \end{aligned} \tag{9}$$

is obtained with the abbreviations:[2]

$$\begin{aligned} m &= \begin{cases} 2n & \text{for } \mathrm{ce}_{2n}, \\ 2n+1 & \text{for } \mathrm{ce}_{2n+1} \text{ and } \mathrm{se}_{2n+1}, \\ 2n+2, & \text{for } \mathrm{se}_{2n+2}, \end{cases} \\ v_m &= \frac{t_v q^2}{a - (m+2)^2 - v_{m+2}}, \qquad n \geq 0 \\ u_m &= \begin{cases} u_0, & n = 0 \\ \dfrac{t_u q^2}{a - (m-2)^2 - u_{m-2}}, & n \geq 1 \end{cases} \end{aligned} \tag{10}$$

where

$$\begin{aligned} t_v &= \begin{cases} 2, & \text{for ce and } v_0 \\ 1, & \text{else} \end{cases} \\ t_u &= \begin{cases} 2, & \text{for ce and } u_2 \\ 1, & \text{else.} \end{cases} \end{aligned} \tag{11}$$

and

$$u_0 = \begin{cases} 0, & \text{for even } m \\ q, & \text{for odd } m \text{ and ce} \\ -q, & \text{for odd } m \text{ and se.} \end{cases}$$

v and u are supplementary variables [7] formulated by the ratio of the corresponding coefficients in (5)–(8), e.g., for (5)

$$\begin{aligned} v_i &= \frac{A_{i+2}}{A_i} \\ u_i &= \frac{A_{i-2}}{A_i}. \end{aligned} \tag{12}$$

The solution of (9) for the first few modes ($m \leq 10$) by usual numerical methods is rather straightforward. For higher mode numbers, however, the following difficulties may arise.

1) For a given value of q there may exist several values of a which can satisfy (9).
2) The expression $L(a)$, (9), is not continuous. It has several poles.
3) The zero of the function $L(a)$ to be determined can be hidden between two poles. A typical function $L(a)$ is shown in Fig. 2(a).

In order to overcome these difficulties, good starting values for a and suitable numerical methods are required. It has turned out that the starting value should deviate from the exact solution by less than 7% for modes $m \leq 10$; for higher-mode numbers m the accuracy of the starting value still has to be increased. So for the mode $m = 300$ the error should be less than 0.3%. In [1], [2], and [7] many good approximations for a can be found, but they are sufficiently accurate only for "small q" or "large q" values. A typical function $a(q)$ is shown in Fig. 2(b). For intermediate values of q (in Fig. 2(b), for instance, between ca. 1000 and 2500), a parabolic approximation has been used by the authors which gives appropriate starting values.

For the standard calculation of the zeros for $L(a)$ (9), the secant method has turned out to be the fastest method in comparison with Muller's, Newton's, and the *regula falsi* method. For the indicated critical cases, a hybrid algorithm has been formulated which starts with the secant method, then applies a type of the bisection method, and ends with the *regula falsi*. This combined algorithm works in both a fast and accurate fashion (at least for 13 reliable, significant digits), for modes $m \leq 300$ and for all positive values of q, which is sufficient for the proposed application.[3]

[1] The separation constant is usually denoted in literature with a [4]; this should not be confused with the semimajor axis a_i [cf. Fig. 1(b)].

[2] This notation, different from that in [7], is common for all modes. This leads merely to one equation (instead of four); the parameters need to be initialized only when the mode changes (t_u, t_v) or at the beginning of the calculation of the value of the functions (v_m, u_m).

[3] For still higher mode numbers, better starting values for a (error $< 0.3\%$) for the "intermediate" values of q have to be chosen.

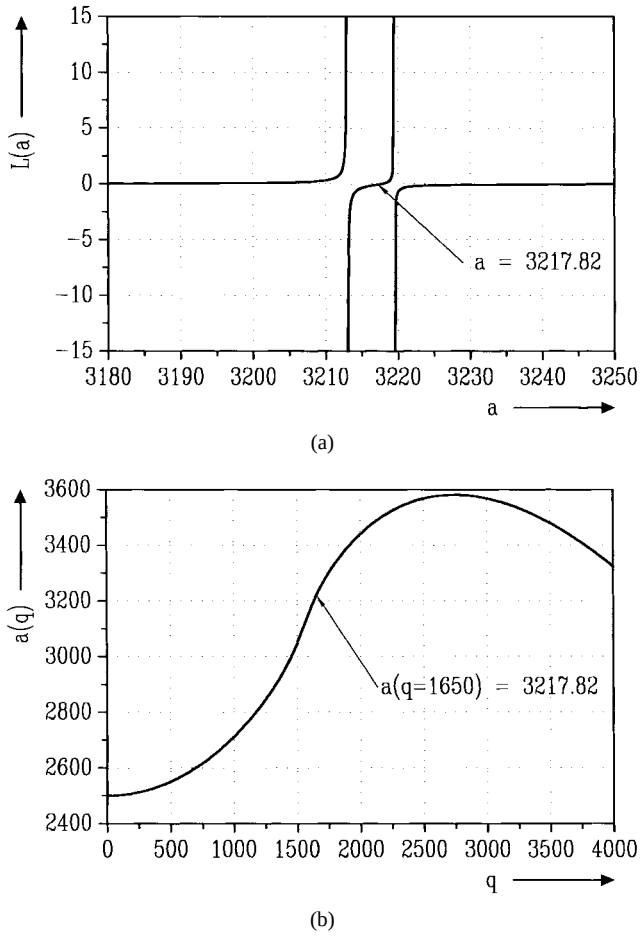

Fig. 2. Determination of the separation constant a, cf., (9). (a) Typical function $L(a)$ (ce, $m = 50$, $q = 1650$). (b) Typical function $a(q)$ ($m = 50$, $q = 1650$).

The consideration of the normalization conditions [7], e.g., for $_{\mathrm{ce}2n}(\eta)$:

$$\int_0^{2\pi} \left[\sum_{r=0}^{\infty} A_{2r} \cos(2rz)\right]^2 dz \stackrel{!}{=} \pi \tag{13}$$

leads to expressions of the form

$$2 + v_0^2 + (v_0 v_2)^2 + (v_0 v_2 v_4)^2 + \cdots = \frac{1}{A_0^2}. \tag{14}$$

From (14), A_0 can be determined. The other coefficients A are then calculated by (10) and (12).

The formal solution of the boundary conditions leads to the following [7]:

$$\begin{Bmatrix} \mathrm{Ce}'(\xi_0, q_c) \\ \mathrm{Se}'(\xi_0, q_c) \end{Bmatrix} = 0, \qquad \text{for TE waves} \tag{15}$$

$$\begin{Bmatrix} \mathrm{Ce}(\xi_0, q_c) \\ \mathrm{Se}(\xi_0, q_c) \end{Bmatrix} = 0, \qquad \text{for TM waves} \tag{16}$$

where q_c are the parametric zeros of the modified Mathieu functions, [cf., also (3)]. With q_c, the cutoff frequencies are given by

$$f_c = \frac{1}{\pi h}\sqrt{\frac{q_c}{\mu\epsilon}} = \frac{c}{\pi h}\sqrt{q_c}. \tag{17}$$

The modes are classified according to increasing cutoff frequencies. The quasi-periodicity of q in (15) and (16) is utilized to calculate the starting values for the next q_c. The accurate value is then calculated with the secant method. This algorithm works reliably for eccentricities $0.001 < e < 0.999$.

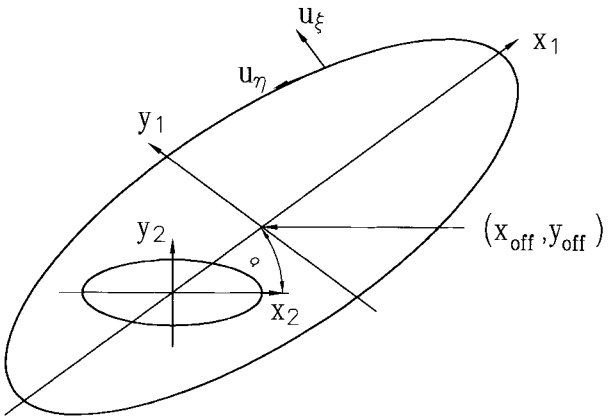

Fig. 3. Coordinate system at the general step discontinuity of elliptical waveguides.

The cutoff frequencies of typical elliptical waveguide cross sections have been calculated up to 300 higher order modes and have been compared with the authors' own finite element method (FEM) calculations and values reported in [8]. Excellent agreement (up to eight digits) has been obtained.

The modal scattering matrix of the general discontinuity (Figs. 1 and 3) is obtained in the usual form [3] by the matching of the tangential field components. Application of the orthogonality of the eigenfunctions and rearranging the equations yields the modal scattering matrix of the discontinuity directly. The normalized matching equations in terms of the eigenmode amplitude coefficients $\boldsymbol{a}$, $\boldsymbol{b}$ of the forward and backward waves, respectively, are given by

$$\boldsymbol{a}_1 + \boldsymbol{b}_1 = [\boldsymbol{M}](\boldsymbol{a}_2 + \boldsymbol{b}_2) \tag{18}$$

$$\boldsymbol{a}_2 - \boldsymbol{b}_2 = [\boldsymbol{M}]^T(\boldsymbol{a}_1 - \boldsymbol{b}_1) \tag{19}$$

where[4]

$$\boldsymbol{M} = \boldsymbol{\delta}_1 \boldsymbol{K} \boldsymbol{\delta}_2 \tag{20}$$

with the diagonal matrices $\boldsymbol{\delta}$ containing the normalization expressions N and the frequency dependent wave impedances and admittances of the adjacent waveguides, respectively.

For elliptical waveguides the following equation was evaluated as a normalization expression:

$$2\pi q \int_0^{\xi_0} \begin{Bmatrix} \mathrm{Ce}^2(\xi) \\ \mathrm{Se}^2(\xi) \end{Bmatrix} [\cosh(2\xi) - X]\, d\xi = \begin{cases} \dfrac{1}{N_i^2 Y_i}, & \text{for TE waves} \\ \dfrac{1}{N_i^2 Z_i}, & \text{for TM waves} \end{cases} \tag{21}$$

where

$$X = \frac{1}{\pi}\int_0^{2\pi} \begin{Bmatrix} \mathrm{ce}^2(\eta) \\ \mathrm{se}^2(\eta) \end{Bmatrix} \cos(2\eta)\, d\eta$$

and Z_i, Y_i, N_i are the wave impedances, admittances, and normalization constant, respectively, of the ith mode classified in increasing cutoff frequency. This expression can be calculated efficiently by merely using the coefficient A_i of the Mathieu functions (see [7]).

[4] the index "1" denotes the larger waveguide, and the index "2" denotes the smaller one.

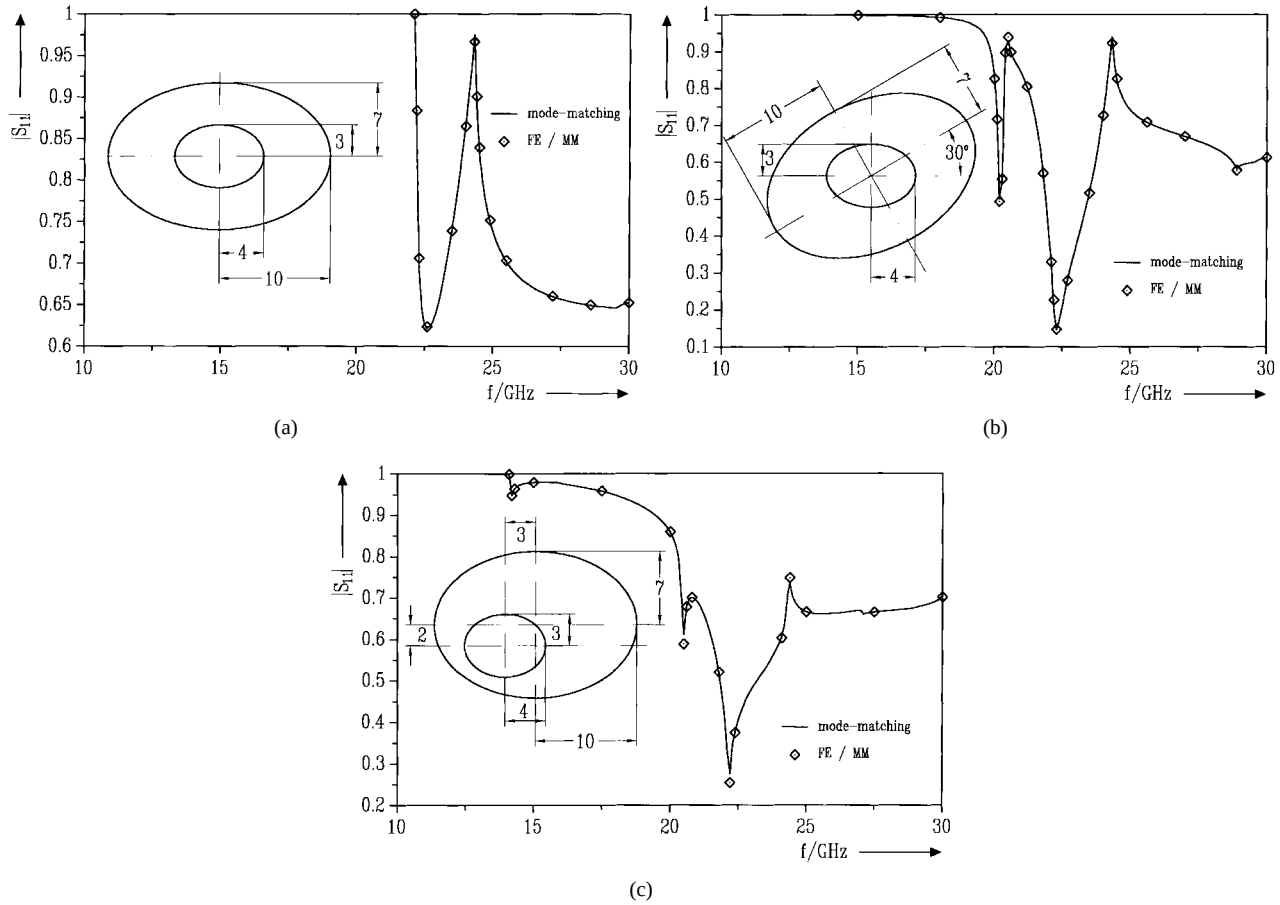

Fig. 4. Input reflection coefficient as a function of frequency (all dimensions in millimeters). (a) Discontinuity of two nonconfocal, concentric elliptic waveguides. (b) Discontinuity of two nonconfocal, twisted elliptic waveguides. (c) Discontinuity of two nonconfocal, displaced elliptic waveguides.

The diagonal matrices $\boldsymbol{\delta}$ are given as follows:

$$\delta_{1i,\,i} = \begin{cases} N_i, & \text{TM wave in the first region} \\ N_i Y_i, & \text{TE wave in the first region} \end{cases} \tag{22}$$

$$\delta_{2i,\,i} = \begin{cases} N_i Z_i, & \text{TM wave in the second region} \\ N_i, & \text{TE wave in the second region.} \end{cases} \tag{23}$$

The general discontinuity of elliptic waveguides is shown in Fig. 3. The coordinate system of the smaller waveguide (index "2") was chosen in this paper as the reference system. The points ξ_2, η_2 of the smaller waveguide are transformed into the coordinates ξ_1 and η_1 via algorithmic expressions. First, from ξ_2 and η_2, x_2 and y_2 are calculated, rotated, and moved, and x_1 and y_1 are obtained. Then ξ_1 and η_1 are calculated by

$$\xi_1 = \operatorname{acosh} \sqrt{\frac{x_1^2 + y_1^2 + h_1^2 + \sqrt{(x_1^2 + y_1^2 + h_1^2)^2 - 4h_1^2 x_1^2}}{2h_1^2}} \tag{24}$$

and

$$\eta_1 = \operatorname{acos} \frac{x_1}{\cosh\, \xi_1}. \tag{25}$$

The coefficients of the coupling matrix $\boldsymbol{K}$ in (20), the coupling integrals $K_{k,\,l}$, are given by expressions like

$$K_{k,\,l} = \iint_{\Omega} \left(\vec{e}_{2l} \times \vec{h}_{1k}\right) d\Omega \tag{26}$$

where $\vec{e}$, $\vec{h}$ are the related vector functions of the cross-sectional form of the mode fields [6]; for the calculation, the surface integral is advantageously transformed via Green's first identity into the corresponding contour integral. The frequency independent coupling integrals for the different mode couplings are explicitly given in the Appendix for the general (nonconfocal, twisted, and displaced) case. For a discontinuity of confocal elliptic waveguides the coupling integrals are given in [5].

With the relation

$$\boldsymbol{b}_2 \underbrace{\left(\boldsymbol{E} + \boldsymbol{M}^T \boldsymbol{M}\right)}_{\boldsymbol{P}} = 2\boldsymbol{M}^T \boldsymbol{a}_1 + \underbrace{\left(\boldsymbol{E} - \boldsymbol{M}^T \boldsymbol{M}\right)}_{\boldsymbol{Q}} \boldsymbol{a}_2$$

the corresponding modal scattering matrix is calculated by

$$\boldsymbol{S}_{11} = 2\boldsymbol{M}\boldsymbol{P}^{-1}\boldsymbol{M}^T - \boldsymbol{E} \tag{27}$$

$$\boldsymbol{S}_{12} = \boldsymbol{M}(\boldsymbol{E} + \boldsymbol{P}^{-1}\boldsymbol{Q}) \tag{28}$$

$$\boldsymbol{S}_{21} = 2\boldsymbol{P}^{-1}\boldsymbol{M}^T \tag{29}$$

$$\boldsymbol{S}_{22} = \boldsymbol{P}^{-1}\boldsymbol{Q}. \tag{30}$$

III. Results

Fig. 4 show the input reflection coefficients as a function of frequency for three discontinuities of two nonconfocal elliptic waveguides; Fig. 4(a) for two concentric waveguides, Fig. 4(b) for two twisted waveguides, and Fig. 4(c) for two displaced waveguides. The results are verified with values obtained by the mode-matching/finite element (MM/FE) method [3]. Excellent agreement may be stated. Results for the confocal case are given in [5].

In order to demonstrate the influence of a twist and a displacement of the elliptic waveguides on the reflection coefficient, Fig. 5 shows the input reflection coefficient as a function of frequency for three different nonconfocal configurations, namely the concentric configuration, the twisted configuration and the twisted/displaced configuration. In all considered configurations, the coupling to the

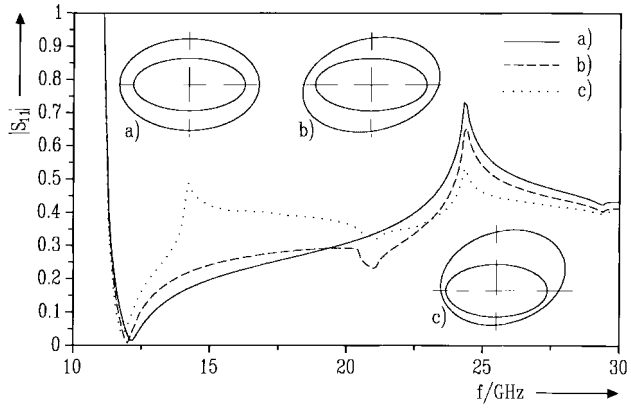

Fig. 5. Input reflection coefficient as a function of frequency for three different nonconfocal configurations. ($a_1 = 10$ mm, $b_1 = 7$ mm, $a_2 = 8$ mm, and $b_2 = 4$ mm). (a) $\alpha = 0°$, $x_{\rm off} = 0$ mm, $y_{\rm off} = 0$ mm. (b) $\alpha = 15°$, $x_{\rm off} = 0$ mm, $y_{\rm off} = 0$ mm. (c) $\alpha = 15°$, $x_{\rm off} = 1$ mm, $y_{\rm off} = 2$ mm.

$E_{s1,\,1}$ mode ($f_c \approx 24.3$ GHz) in the first waveguide causes a peak at approximately 24.3 GHz. In the second configuration, the coupling to the $E_{c1,\,1}$ mode ($f_c \approx 20.4$ GHz) in the first waveguide causes the discontinuance at approximately 20.4 GHz, the coupling to the $H_{s1,\,1}$ mode ($f_c \approx 21.0$ GHz) in the second waveguide causes the minimum at approximately 21.0 GHz. In the third configuration, the coupling to the $E_{c0,\,1}$ mode ($f_c \approx 14.2$ GHz) in the first waveguide causes a peak at approximately 14 GHz.

For the calculations, all higher-order modes in the order of increasing cutoff are considered up to the cutoff frequency of 100 GHz. The efficiency of the presented method may be demonstrated by the fact that the above direct mode-matching results are calculated by using a very simple 486-level PC (20 MHz, peak performance ca. 0.2 MFlops), at which the overall central processing unit (CPU) time for a typical frequency response with 1000 frequency points was approximately 600 min. The most significant part of the CPU time was used for solving the eigenvalue problem. The maximum accuracy (up to 13 digits) has been utilized in this case and the program has not yet been optimized. The reference calculations in Fig. 4 with the hybrid MM/FE method [3] took about 30 min on an IBM SP2 workstation (peak performance 260 MFlops). Therefore, the direct mode-matching technique presented in this paper may be roughly estimated to be about 65 times faster than the MM/FE method [3] which is, for its part, already ca. one order of magnitude faster than a usual three-dimensional (3-D) FEM.

IV. Conclusion

In this paper, a direct mode-matching technique was proposed for the calculation of the modal scattering matrix of the general (nonconfocal, displaced, twisted) step discontinuity of elliptical waveguides. Due to the high numerical efficiency of the method, only a standard PC is required for the rigorous analysis of the investigated discontinuities.

Appendix

The coupling integrals in (20) and (26) for the general case (Figs. 1 and 3) are given in the following equation.[5]

[5] All Mathieu functions depend (aside from the coordinate parameter) upon the mode m and parameter q, which can be evaluated from the wave mode number and wave cutoff frequency of the appropriate waveguide. To make the equations more readable only the indexs "1" and "2" are used to indicate the waveguide to which the Mathieu functions are related.

For all four types of TE–TE couplings; for $k_{c1} \neq k_{c2}$:

$$K_{k,\,l} = \frac{k_{c2}^2}{k_{c2}^2 - k_{c1}^2} \begin{Bmatrix} \mathrm{Ce}_2\,(\xi_0) \\ \mathrm{Se}_2\,(\xi_0) \end{Bmatrix} \times \int_0^{2\pi} \frac{G_2}{G_1} \times \begin{Bmatrix} \mathrm{Ce}_1'\,(\xi_1)\mathrm{ce}_1\,(\eta_1)\vec{u}_{\xi_1} + \mathrm{Ce}_1\,(\xi_1)\mathrm{ce}_1'\,(\xi_1)\vec{u}_{\eta_1} \\ \mathrm{Se}_1'\,(\xi_1)\mathrm{se}_1\,(\eta_1)\vec{u}_{\xi_1} + \mathrm{Se}_1\,(\xi_1)\mathrm{se}_1'\,(\eta_1)\vec{u}_{\eta_1} \end{Bmatrix} \times \begin{Bmatrix} \mathrm{ce}_2\,(\eta_2) \\ \mathrm{se}_2\,(\eta_2) \end{Bmatrix} \vec{u}_{\xi_2}\, d\eta_2 \tag{31}$$

otherwise

$$K_{k,\,l} = \int_0^{\xi_0} \int_0^{2\pi} \frac{1}{G_1} \times \begin{Bmatrix} \mathrm{Ce}_1'\,(\xi_1)\mathrm{ce}_1\,(\eta_1)\vec{u}_{\xi_1} + \mathrm{Ce}_1\,(\xi_1)\mathrm{ce}_1'\,(\eta_1)\vec{u}_{\eta_1} \\ \mathrm{Se}_1'\,(\xi_1)\mathrm{se}_1\,(\eta_1)\vec{u}_{\xi_1} + \mathrm{Se}_1\,(\xi_1)\mathrm{se}_1'\,(\eta_1)\vec{u}_{\eta_1} \end{Bmatrix} \times \begin{Bmatrix} \mathrm{Ce}_2'\,(\xi_2)\mathrm{ce}_2\,(\eta_2)\vec{u}_{\xi_2} + \mathrm{Ce}_2\,(\xi_2)\mathrm{ce}_2'\,(\eta_2)\vec{u}_{\eta_2} \\ \mathrm{Se}_2'\,(\xi_2)\mathrm{se}_2\,(\eta_2)\vec{u}_{\xi_2} + \mathrm{Se}_2\,(\xi_2)\mathrm{se}_2'\,(\eta_2)\vec{u}_{\eta_2} \end{Bmatrix} \times d\eta_2\, d\xi_2. \tag{32}$$

For all four types of TM–TM couplings; for $k_{c1} \neq k_{c2}$:

$$K_{k,\,l} = \frac{k_{c1k}^2}{k_{c1k}^2 - k_{c2l}^2} \begin{Bmatrix} \mathrm{Ce}_2'\,(\xi_0) \\ \mathrm{Se}_2'\,(\xi_0) \end{Bmatrix} \times \int_0^{2\pi} \begin{Bmatrix} \mathrm{ce}_2\,(\eta_2) \\ \mathrm{se}_2\,(\eta_2) \end{Bmatrix} \begin{Bmatrix} \mathrm{Ce}_1\,(\xi_1)\mathrm{ce}_1\,(\eta_1) \\ \mathrm{Se}_1\,(\xi_1)\mathrm{se}_1\,(\eta_1) \end{Bmatrix} d\eta_2 \tag{33}$$

otherwise (33).[6]

For all four types of the TM–TE couplings:

$$K_{k,\,l} = \begin{Bmatrix} \mathrm{Ce}_2\,(\xi_0) \\ \mathrm{Se}_2\,(\xi_0) \end{Bmatrix} \times \int_0^{2\pi} \begin{bmatrix} \mathrm{Ce}_1\,(\xi_1)\mathrm{ce}_1\,(\eta_1) \\ \mathrm{Se}_1\,(\xi_1)\mathrm{se}_1\,(\eta_1) \end{bmatrix} \begin{Bmatrix} \mathrm{ce}_2'\,(\eta_2) \\ \mathrm{se}_2'\,(\eta_2) \end{Bmatrix} d\eta_2. \tag{34}$$

For all four types of the TE–TM couplings

$$K_{k,\,l} = 0. \tag{35}$$

In these equations the dash denotes the corresponding derivative, ξ_0 is the boundary coordinate of the smaller waveguide, and

$$G_i = h_i \sqrt{\cosh^2(\xi_i) - \cos^2(\eta_i)}$$

is Lamé's factor of the transformation.

Acknowledgment

The authors wish to thank R. Beyer for many discussions and for the MM/FE reference calculations.

References

[1] M. Abramowitz and I. A. Stegun, *Handbook of Mathematical Functions.* New York: Dover, 1970.
[2] F. M. Arscott, *Periodic Differential Equations.* London, U.K.: Pergamon, 1964.
[3] R. Beyer and F. Arndt, "Efficient modal analysis of waveguide filters including the orthogonal mode coupling elements by an MM/FE method," *IEEE Microwave Guided Wave Lett.*, vol. 5, pp. 9–11, Jan. 1995.
[4] D. A. Goldberg, L. J. Laslett, and R. A. Rimmer, "Modes of elliptical waveguides: A correction," *IEEE Trans. Microwave Theory Tech.*, vol. 38, pp. 1603–1608, Dec. 1990.
[5] P. Matras, R. Bunger, and F. Arndt, "Mode-matching analysis of the step discontinuity in elliptical waveguides," *IEEE Microwave Guided Wave Lett.*, vol. 6, pp. 143–145, Mar. 1996.
[6] N. Marcuvitz, *Waveguide Handbook.* New York: McGraw-Hill, 1951, pp. 80–84.

[6] Note that the different parameters q of the Mathieu functions are the only difference between (33) for the TE–TE and TM–TM couplings, respectively, in this case.

[7] N. W. McLachlan, *Theory and Application of Mathieu Functions.* New York: Dover, 1964.
[8] B. K. Wang, K. Y. Lam, M. S. Leong, and P. S. Kooi, "Elliptical waveguide analysis using improved polynomial approximation," *Proc. Inst. Elec. Eng.*, vol. 141, pt. H, pp. 483–488, Dec. 1994.

Dispersion Characteristics of Open Microstrip Lines Using Closed-Form Asymptotic Extraction

Seong-Ook Park and Constantine A. Balanis

***Abstract*— A full-wave spectral-domain method with an asymptotic extraction technique is formulated for multilayer microstrip lines. This formulation provides a simple closed-form representation of the asymptotic part of the impedance matrix by using Chebyshev polynomial basis functions with the square-root edge condition and the asymptotic behavior of the Green's function. The formulation is applied to open microstrip lines. Numerical results, in the form of the effective dielectric constants, are presented for the dominant mode. It is shown that the proposed method significantly reduces the computational time and improves the accuracy over the conventional spectral-domain approach (SDA).**

***Index Terms*—Accleration technique, microstrip lines, spectral-domain approach.**

I. Introduction

The spectral-domain approach (SDA) is the most popular technique for calculating the dispersion characteristics of open microstrip lines [1] because it is easy to formulate and is a rigorous full-wave solution for simple and uniform planar structures. The SDA has been extensively studied and refined to find well-suited basis functions that have the ability to accurately represent and resemble the longitudinal and transverse current densities (J_z and J_x) while minimizing the computation time [2]–[5].

However, there are still slight discrepancies of the relative effective permittivity between many numerical results obtained by various methods [6]. These discrepancies are critically dependent on the type of basis functions used and the truncation error due to the finite upper limit (instead of infinity) for the numerical integration in the evaluation of the impedance matrix elements. Although the basis functions are carefully chosen to effectively represent the expected current densities, lengthy computation time is required for the numerical integration in the evaluation of the impedance matrix elements to achieve the desired accuracy.

In this paper, as one possible technique for overcoming this, the authors present a closed form for the asymptotic part of the spectral impedance matrix to evaluate the relative effective permittivity in single conductor, open microstrip lines. Using the asymptotic technique, the asymptotic part of impedance matrix elements is recognized as being integrable in closed form by introducing Chebyshev polynomial basis functions with the square-root edge condition.

Manuscript received February 29, 1996; revised November 21, 1996. This work is based upon work supported by the U.S. Army Research Office under Grant DAAL03-92-G-0262.

The authors are with the Department of Electrical Engineering, Telecommunications Research Center, Arizona State University, Tempe, AZ 85287-7206 USA.

Publisher Item Identifier S 0018-9480(97)01713-4.

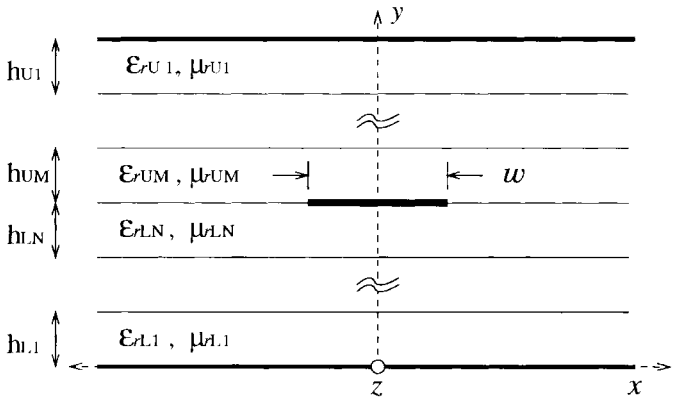

Fig. 1. Geometry of a multilayer microstrip line structure.

To verify the accuracy and speed of the proposed method, computations based on this method were compared with other available results. There is good agreement between the proposed method and other available methods. The proposed method significantly reduces the central processing unit (CPU) time and increases the reliability and accuracy.

II. Closed-Form Asymptotic Extraction of the Spectral-Domain Green's Function

The cross section of a general planar microstrip structure is shown in Fig. 1. The strip conductor is assumed to be negligibly thin and the line lossless. The substrate and superstrate materials are lossless and isotropic. The open microstrip lines in [4] can be accurately modeled by letting $h_{UM} \to \infty$, considering only one substrate and superstrate in Fig. 1. To calculate the effective dielectric constant (dispersion characteristic), the proposed method in this paper is formulated to include any number of substrate or superstrate structures. However, to verify the authors' method, an open microstrip line is used and the results are compared with previously published data [3], [4], [6].

As an initial step to investigate the asymptotic closed-form extraction for the impedance matrix elements, the authors extract the asymptotic behavior of the Green's function, with respect to α. Assuming that α is sufficiently large, one can make the following approximation:

$$\gamma_i = \sqrt{\alpha^2+\beta^2-k_i^2} \simeq |\alpha|, \qquad \text{if } \alpha^2 \gg (\epsilon_{\text{reff}}-\epsilon_{ri})k_0^2 \quad (1)$$

$$\coth(\gamma_i h_i) \simeq \coth(|\alpha| h_i) \simeq 1, \qquad \text{if } |\alpha| h_i > 3 \quad (2)$$

$$\alpha^2+\beta^2 \simeq \alpha^2 \quad (3)$$

where α, β, and γ_i are the wavenumbers in the $\hat{x}$, $\hat{z}$, and $\hat{y}$ directions, respectively [1].

Since (2) is in error by about 0.5% for $|\alpha| h_i = 3$, $\coth(|\alpha| h_i) \simeq 1$ is a good approximation for $|\alpha| h_i > 3$. Using the above approximations, asymptotic expressions of the recurrence Green's function in [7] can be derived as follows [after correcting for the misprints in [7] where $\alpha_{y(j)}^2/\mu_{r(j)}^2$ is replaced by $\epsilon_{r(j)}^2/\alpha_{y(j)}^2$ in (9a) and $\epsilon_{r(j)}^2/\alpha_{y(j)}^2$ is replaced by $\alpha_{y(j)}^2/\mu_{r(j)}^2$ in (9b)]:

$$\tilde{G}_{zz}^{\infty} \simeq \frac{1}{|\alpha|}\left[\frac{\beta^2}{\epsilon_{rLN}+\epsilon_{rUM}} - k_0^2 \frac{\mu_{rLN}\mu_{rUM}}{\mu_{rLN}+\mu_{rUM}}\right] \quad (4)$$

$$\tilde{G}_{xx}^{\infty} \simeq \frac{|\alpha|}{\epsilon_{rLN}+\epsilon_{rUM}} \quad (5)$$

$$\tilde{G}_{xz}^{\infty} \simeq \left(\frac{\beta}{\epsilon_{rLN}+\epsilon_{rUM}}\right) \cdot \text{sgn}(\alpha) \quad (6)$$